Supporting Information

Computational and Experimental Identification of Strong Synergy of Fe/ZnO Catalyst in Promoting Acetic Acid Synthesis from CH_4 and CO_2

Xiaowa Nie,*[#,a,b] Xianxuan Ren,[#,a] Chunyan Tu,[#,b] Chunshan Song,[a,c] Xinwen Guo*[a] and Jingguang G. Chen*[b]

[a] State Key Laboratory of Fine Chemicals, PSU-DUT Joint Center for Energy Research, and School of Chemical Engineering, Dalian University of Technology, Dalian, Liaoning 116024, P.R. China

[b] Department of Chemical Engineering, Columbia University, New York, NY 10027, USA

[c] EMS Energy Institute, PSU-DUT Joint Center for Energy Research, and Department of Energy & Mineral Engineering, Pennsylvania State University, University Park, PA 16802, USA

[#] These authors contributed equally to this work.

1. Computational Methods

Spin polarized density functional theory (DFT) calculations were performed using the Vienna Ab Initio Simulation Pack-age (VASP).[1] The Perdew-Burke-Ernzerhof (PBE) functional based on generalized gradient approximation (GGA) was utilized to compute the exchange and correlation energies.[2] The projector-augmented wave (PAW) potentials were employed to describe the effective ion cores[3] and a plane wave basis set with a cutoff energy of 400 eV was used. Structural optimization was conducted using the damped molecular dynamics method and the convergence criterion for maximum force on each atom was set to 0.02 eV/Å. In order to improve the local accuracy of the Zn 3d states, the DFT+U method was utilized with a Hubbard parameter set to 5.0 eV, consistent with previous theoretical studies on ZnO-involved systems.[4] Dispersion corrections were considered for weakly adsorbed species by using the PBE+D3 method.[5] To map out the potential energy surface, the climbing image

nudged elastic band (CI-NEB) method was used to search transition states,[6] which were confirmed to have a single imaginary vibrational frequency along the reaction coordinate via vibrational frequency calculations. Bader charge calculation was performed based on the code developed by Henkelman and co-workers.[7]

For bulk ZnO, the calculated lattice parameters are a = b = 3.28 Å and c = 5.29 Å, in reasonable agreement with experimental values.[8] The band gap calculated for bulk ZnO using PBE+$U_{5.0}$ was 0.92 eV, which was lower than the experimentally determined value (~3.3 eV)[9] but was consistent with the value range (0.7~0.9 eV) reported in DFT studies using PBE functional in the literature.[10-14] To examine the effect of computational methods on the band gap of ZnO as well as on the charge transfer, surface adsorption and reaction on ZnO, different computational methods were employed including PBE+$U_{7.5}$, PW91+$U_{5.0}$ and rPBE+$U_{5.0}$. The calculation results were provided in **Table S1**, which showed that the band gap calculated using different methods were all lower than the experimental value. However, for the charge transfer associated with the CH_4 dissociation step, the differences among these methods were small. Furthermore, the effect of electronic structure methods examined on the adsorption and surface reactivity of CH_4 dissociation was not significant, showing weak adsorption and slow dissociation on the ZnO support. Therefore, the PBE+$U_{5.0}$ method was used throughout the work. In this work, the non-polar ZnO($10\bar{1}0$) was selected as the surface model, which has shown good activity in heterogeneous catalytic reactions.[15] A *p*(3×2) supercell containing six atomic layers of ZnO($10\bar{1}0$) was constructed, the bottom two atomic layers of which were fixed at their original bulk positions while the top four layers together with adsorbates were fully relaxed during geometric optimization. A 15 Å of vacuum space was included to avoid interactions between repeating slabs. A k-point sampling of 2×2×1 within the Monk-horst−Pack scheme was used for all surface calculations. All possible sites for Fe location on ZnO($10\bar{1}0$) were examined, including substituting Zn and O atoms at different locations, as well as binding above the ZnO($10\bar{1}0$) surface, as illustrated in **Figure S2(a)**. The adsorption of CH_4 was examined on these Fe/ZnO surfaces, and the energetically most favorable CH_4 adsorption was found to be the Fe substituting an O_c atom, which had an adsorption energy of -0.37 eV, more stable than that adsorbed at other Fe locations (see **Figure S2(b)**). Same favorable Cu location was used to construct the Cu/ZnO($10\bar{1}0$) surface, in which a Cu atom

substituted the Oc atom on ZnO($10\bar{1}0$). The adsorption energy is defined as:

$$\boldsymbol{E_{ads} = E_{(adsorbate\text{-}surface)} - E_{(adsorbate)} - E_{(bare\ surface)}}$$

Where $E_{(adsorbate\text{-}surface)}$ is the total energy of adsorbed species with the surface slab, $E_{(adsorbate)}$ represents the energy of adsorbate in gas phase, and $E_{(bare\ surface)}$ is the energy of unoccupied surface. Zero point energy, heat capacity, and entropy were computed with standard methods and then used to convert the electronic energies into Gibbs free energies at the temperature of 673 K.

Figure S1 reveals that at 1 bar, although the production of acetic acid is enhanced with increasing reaction temperature, the equilibrium amount of acetic acid is still very low. A noteworthy enhancement of acetic acid production can be achieved when the pressure is increased (e.g. 30 bar) along with a temperature that is not very high (e.g. 573 K). Therefore, both efficient catalysts and optimized reaction conditions are essential for improving the yield of acetic acid.

2. Experimental Methods

2.1 Catalysts Synthesis

The Fe/ZnO and Cu/ZnO catalysts were prepared by deposition-precipitation on the ZnO powder support (Sigma-Aldrich, S_{BET} 15~25m^2/g), using $Fe(NO_3)_3 \cdot 9H_2O$ (Sigma-Aldrich) and $Cu(NO_3)_2 \cdot 3H_2O$ (Sigma-Aldrich) as the precursor, respectively. The ZnO support was added into an aqueous solution (25 mL) with the desired amount of iron nitrate or copper nitrate. The resulting suspension was stirred vigorously at 333 K for 60 min. Then, 0.2 mol/L of ammonia carbonate ($(NH_4)_2CO_3$ from Sigma-Aldrich) aqueous solution was added dropwise into the above mixture until pH 9.0 was achieved. After vigorously stirring at 333 K for 120 min, the solution pH remained almost constant. The resulting slurry was filtered and washed thoroughly with deionized water. The obtained solids were dried at 373 K for 6 h and then calcinated in air at 673 K for 2 h. The Fe or Cu loading of these catalysts was 5 wt %.

2.2 In-situ Diffuse Reflectance Infrared Fourier Transform Spectroscopy Tests

In situ DRIFTS tests were conducted on an FTIR spectrometer (Thermo Fisher, Nicolet

6700) with an MCT detector. Before measurement, the catalyst (Fe/ZnO or Cu/ZnO) was firstly reduced in 50%H_2/ 50%He (10 mL/min) at 773 K for 60 min and then purged with He (10 mL/min) at 500 ℃ for 60 min. ZnO support was pretreated in He flow (10 mL/min) at 773 K. Subsequently, the sample was cooled down to 673 K, and the background spectrum was collected at 673 K in He flow (10 mL/min). The CH_4+CO_2 reaction was performed in a mixture of 30%CO_2/30%CH_4/40%He (10 mL/min) at 673 K for 60 min. Afterwards, the reaction cell was purged with He (10 mL/min) for 30 min. The in situ DRIFT spectra were recorded by collecting 32 scans at a resolution of 4 cm^{-1}.

To further study the intermediates during the CH_4+CO_2 reaction over Fe/ZnO, a "CH_4 off−CH_4 on" test was also performed. After the reduction pretreatment, as described above, the spectra were recorded according to the following steps. First, the reduced Fe/ZnO catalyst was exposed to 30%CO_2/70%He (10 mL/min) at 673 K for 30 min. Then, we introduced CH_4 into the gas stream, keeping the catalyst in a gas mixture of 30%CO_2/30%CH_4/40%He (10 mL/min) for 30 min. After this, He (10 mL/min) was flowed over the catalyst for 30 min.

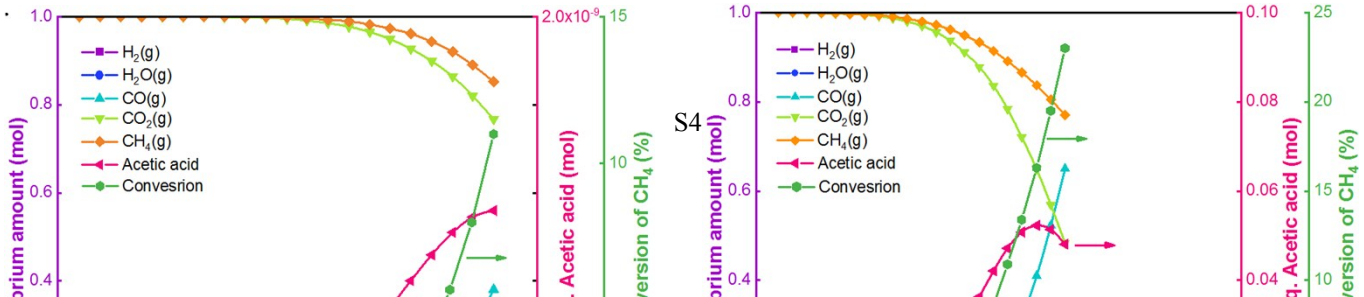

(a) **(b)**

Figure S1. The calculated equilibrium amount of acetic acid formation from conversion of CO_2 and CH_4 as a function of temperature at (a) 1 bar and (b) 30 bar. (Conditions: feed ratio: CO_2(g)/CH_4(g)=1 mol/1 mol; temperature range: 25-350/500℃; involved reactions: acetic acid formation, reforming and reverse water gas shift.). The thermodynamic equilibrium values were calculated using HSC Chemistry 6.0.

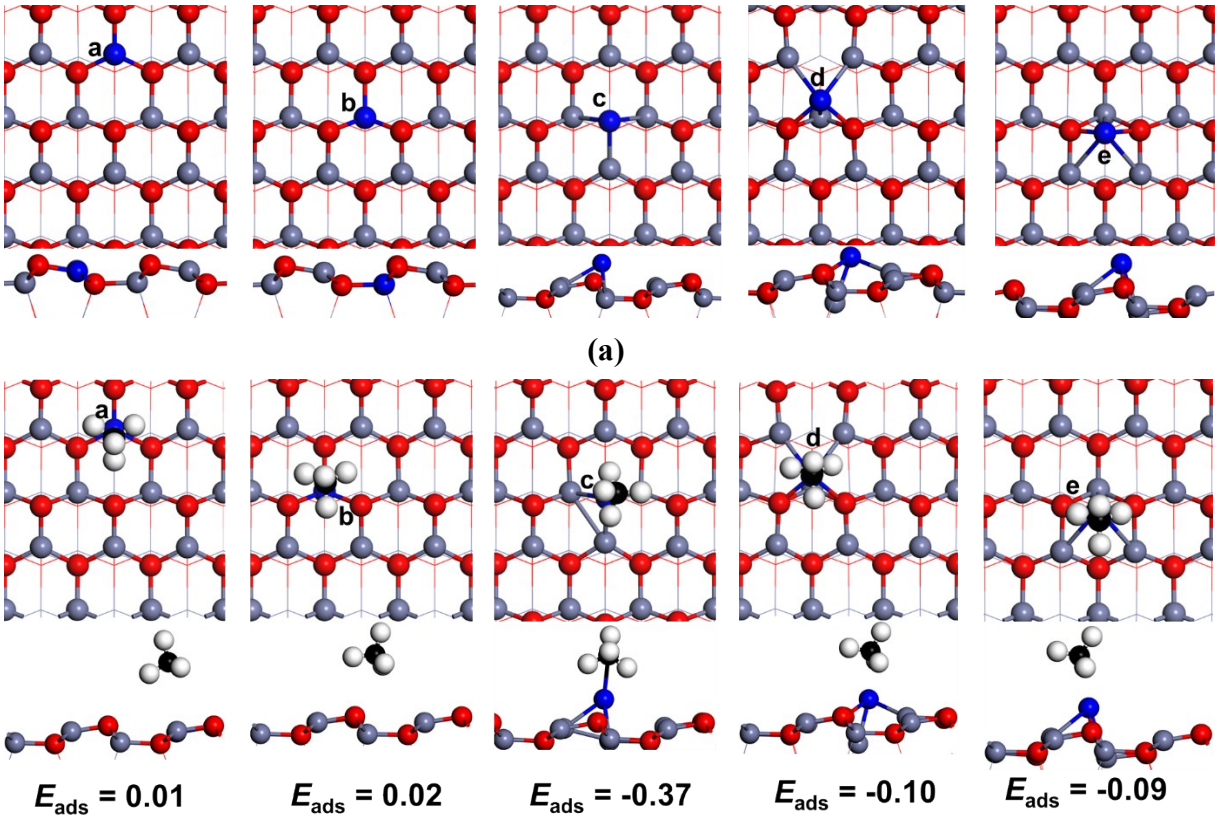

Figure S2. (a) Different Fe locations on ZnO($10\bar{1}0$) including substituting Zn_a and Zn_b, substituting O_c and O_d, as well as binding above the ZnO surface. (b) CH_4 adsorption configurations and energies on Fe/ZnO($10\bar{1}0$) with different Fe locations.

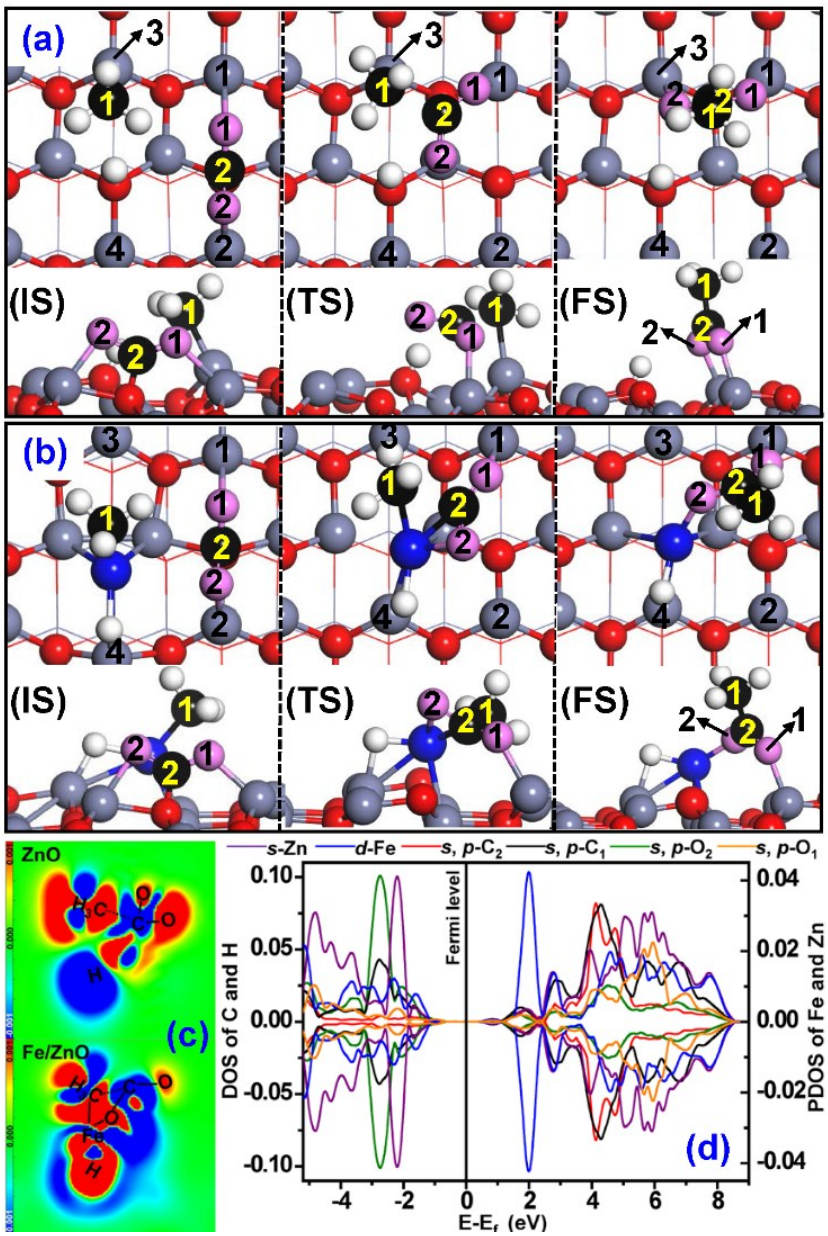

Figure S3. Optimized structures of initial, transition and final states associated with C-C coupling of CO_2* with M-CH_3* on (a) ZnO($10\bar{1}0$) and (b) Fe/ZnO($10\bar{1}0$) surfaces (grey: Zn, blue: Fe, red: O of ZnO, pink: O of CO_2, black: C, white: H). (c) Electron density difference maps of transition states for C-C coupling on the two surfaces. (d) DOS and PDOS of transition state for C-C coupling on Fe/ZnO($10\bar{1}0$).

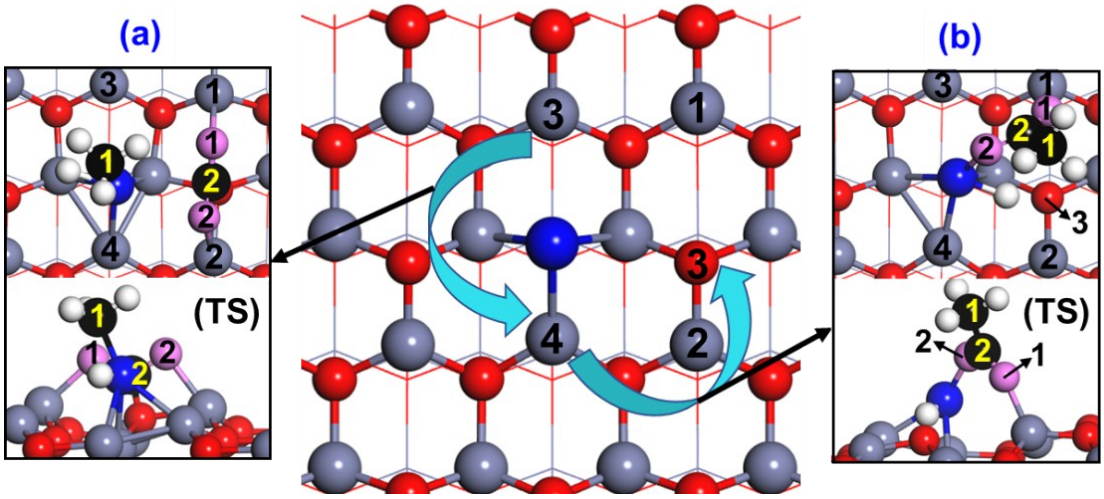

Figure S4. Structural illustrations of transition states associated with H_{diss} migration from (a) the initial Zn_3…Fe to Zn_4…Fe bridge site and (b) the Zn_4…Fe bridge site to surface O_3 site on Fe/ZnO($10\bar{1}0$) surface (grey: Zn, blue: Fe, red: O of ZnO, pink: O of CO_2, black: C, White: H).

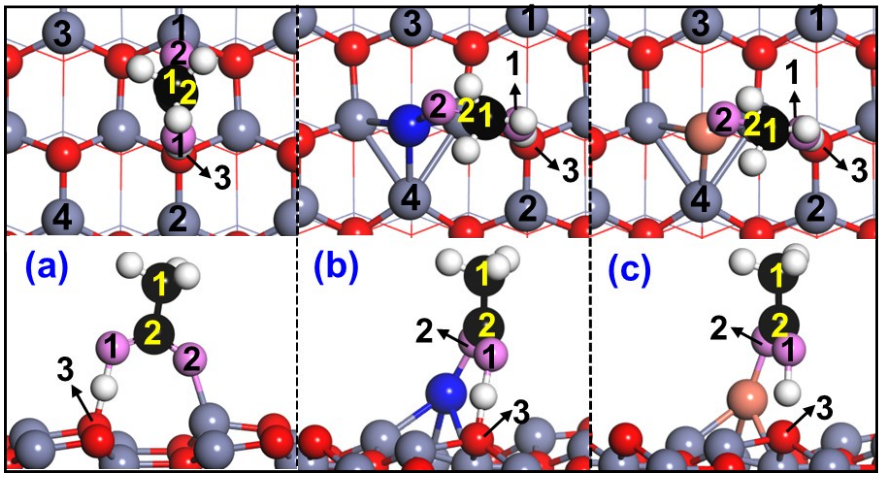

Figure S5. Optimized structures of adsorbed acetic acid on (a) ZnO($10\bar{1}0$), (b) Fe/ZnO($10\bar{1}0$) and (c) Cu/ZnO($10\bar{1}0$) surfaces (grey: Zn, orange: Cu, blue: Fe, red: O of ZnO, pink: O of CO_2, black: C, White: H).

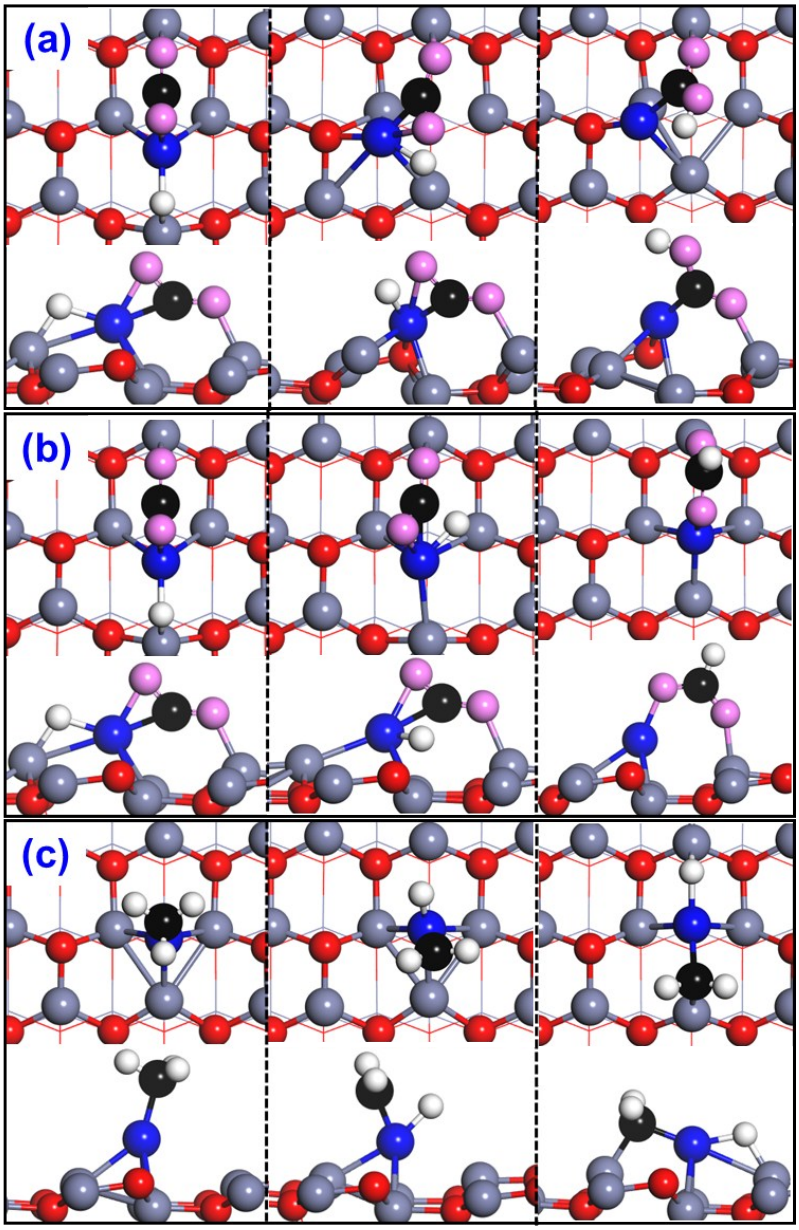

Figure S6. Optimized structures of initial, transition, and final states associated with CO_2* hydrogenation to (a) COOH* and (b) HCOO* intermediates, as well as (c) CH_3* dissociation to CH_2*+H* on Fe/ZnO($10\bar{1}0$) surface (grey: Zn, blue: Fe, red: O of ZnO, pink: O of CO_2, black: C, White: H).

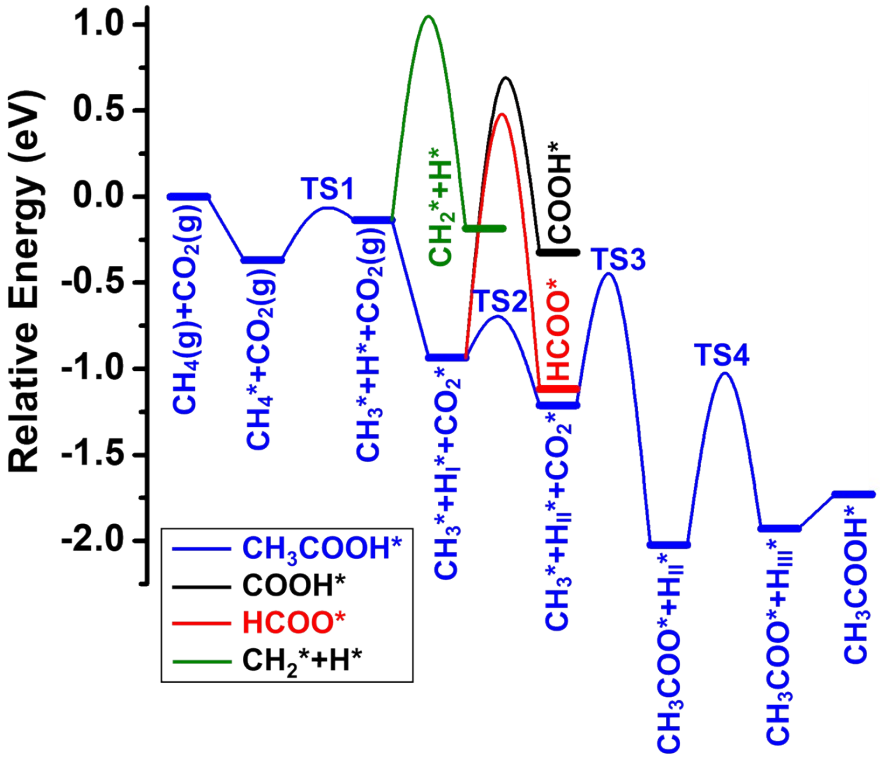

Figure S7. Energy profiles of acetic acid formation from CO_2 and CH_4 as well as side reactions including CO_2* hydrogenation to HCOO* and COOH* intermediates and CH_3* dissociation to CH_2*+H* on Fe/ZnO($10\bar{1}0$) surface (H_I* denotes the initial H_{diss} site from CH_4 dissociation, H_{II}* represents the first H_{diss} migration from the initial Zn_3…M to Zn_4…M bridge site, and H_{III}* stands for the second H_{diss} migration from the Zn_4…M bridge site to surface O_3 site).

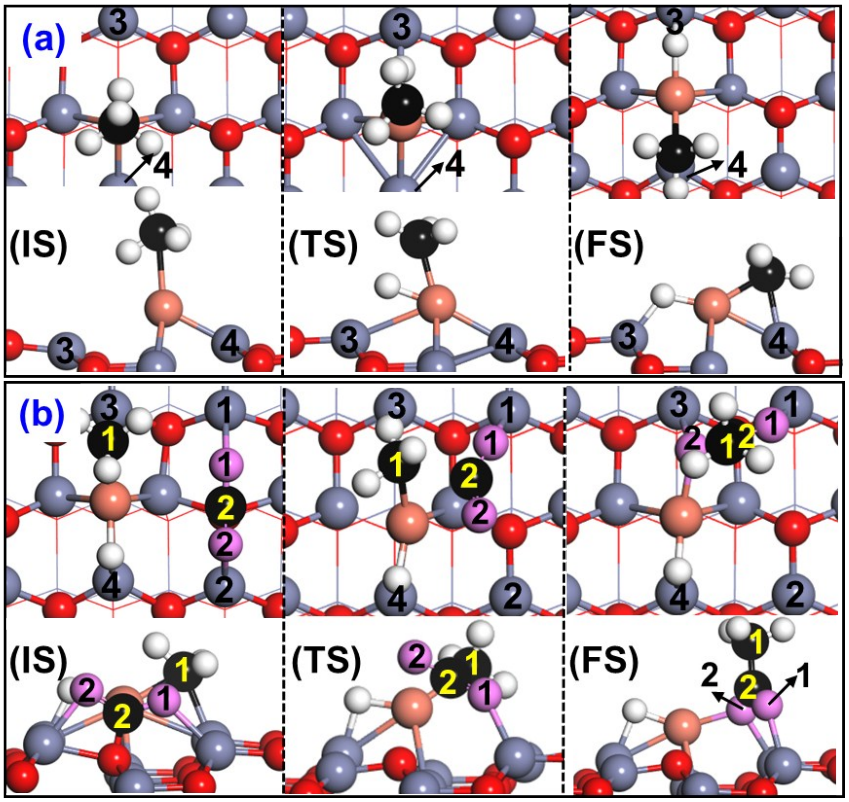

Figure S8. Optimized structures of initial, transition and final states associated with (a) CH_4 dissociation and (b) C-C coupling on Cu/ZnO($10\bar{1}0$) surface (grey: Zn, orange: Cu, red: O of ZnO, pink: O of CO_2, black: C, White: H).

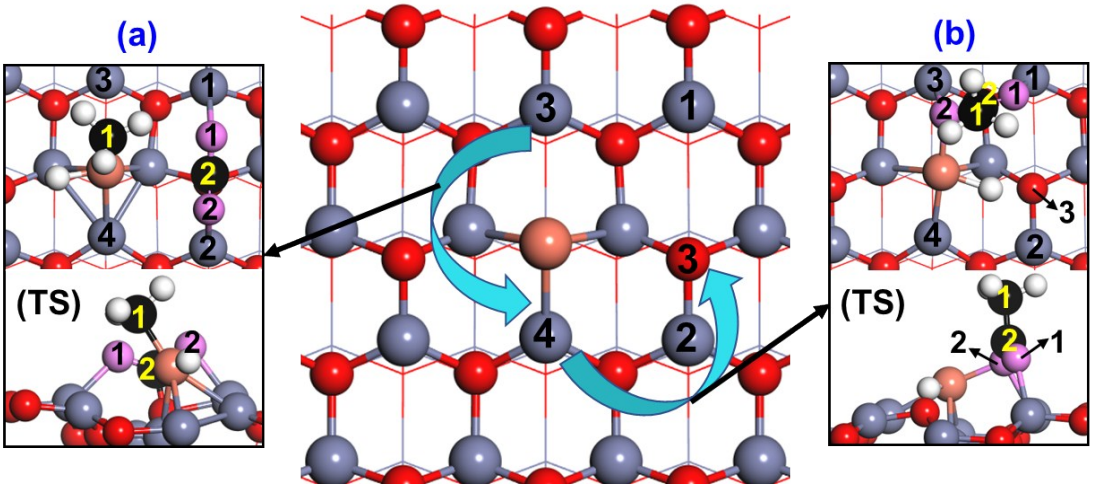

Figure S9. Structural illustrations of transition states associated with H_{diss} migration from (a) the initial Zn_3…Cu to Zn_4…Cu bridge site and (b) the Zn_4…Cu bridge site to surface O_3 site on Cu/ZnO($10\bar{1}0$) surface (grey: Zn, orange: Cu, red: O of ZnO, pink: O of CO_2, black: C,

White: H).

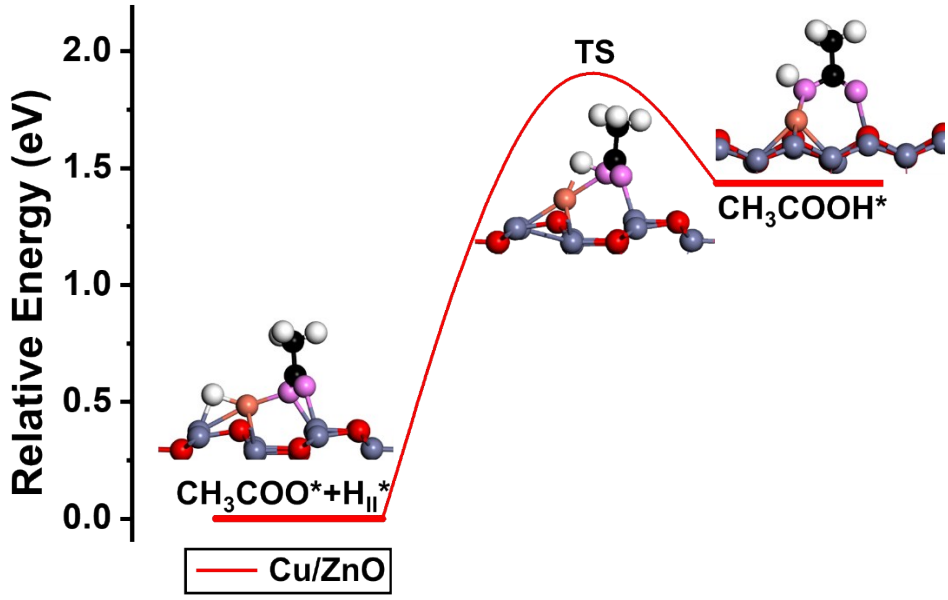

Figure S10. The energy diagram of direct hydrogenation of acetate to form acetic acid with H_{diss} adsorbed at the Zn_4…Cu bridge site on Cu/ZnO($10\bar{1}0$).

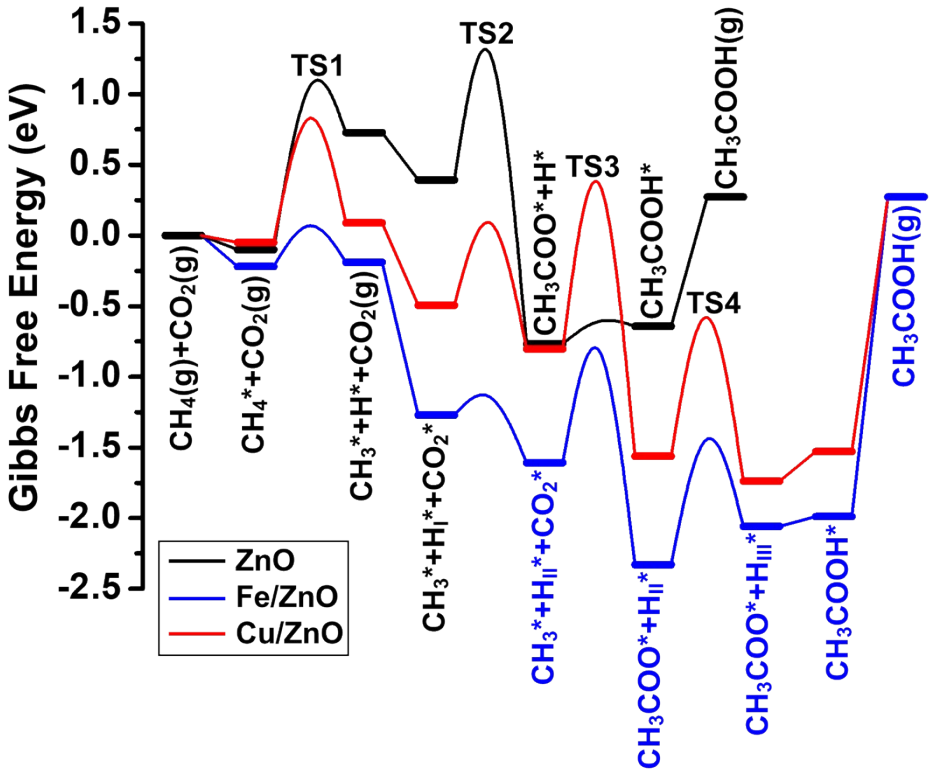

Figure S11. Energy profiles based on Gibbs free energies for acetic acid synthesis from CO_2 and CH_4 on ZnO($10\bar{1}0$) (black line), Fe/ZnO($10\bar{1}0$) (blue line) and Cu/ZnO($10\bar{1}0$) (red line)

surfaces at 673 K (H_I* denotes the initial H_{diss} site from CH_4 dissociation, H_{II}* represents the first H_{diss} migration from the initial Zn_3…M to Zn_4…M bridge site, and H_{III}* stands for the second H_{diss} migration from the Zn_4…M bridge site to surface O_3 site).

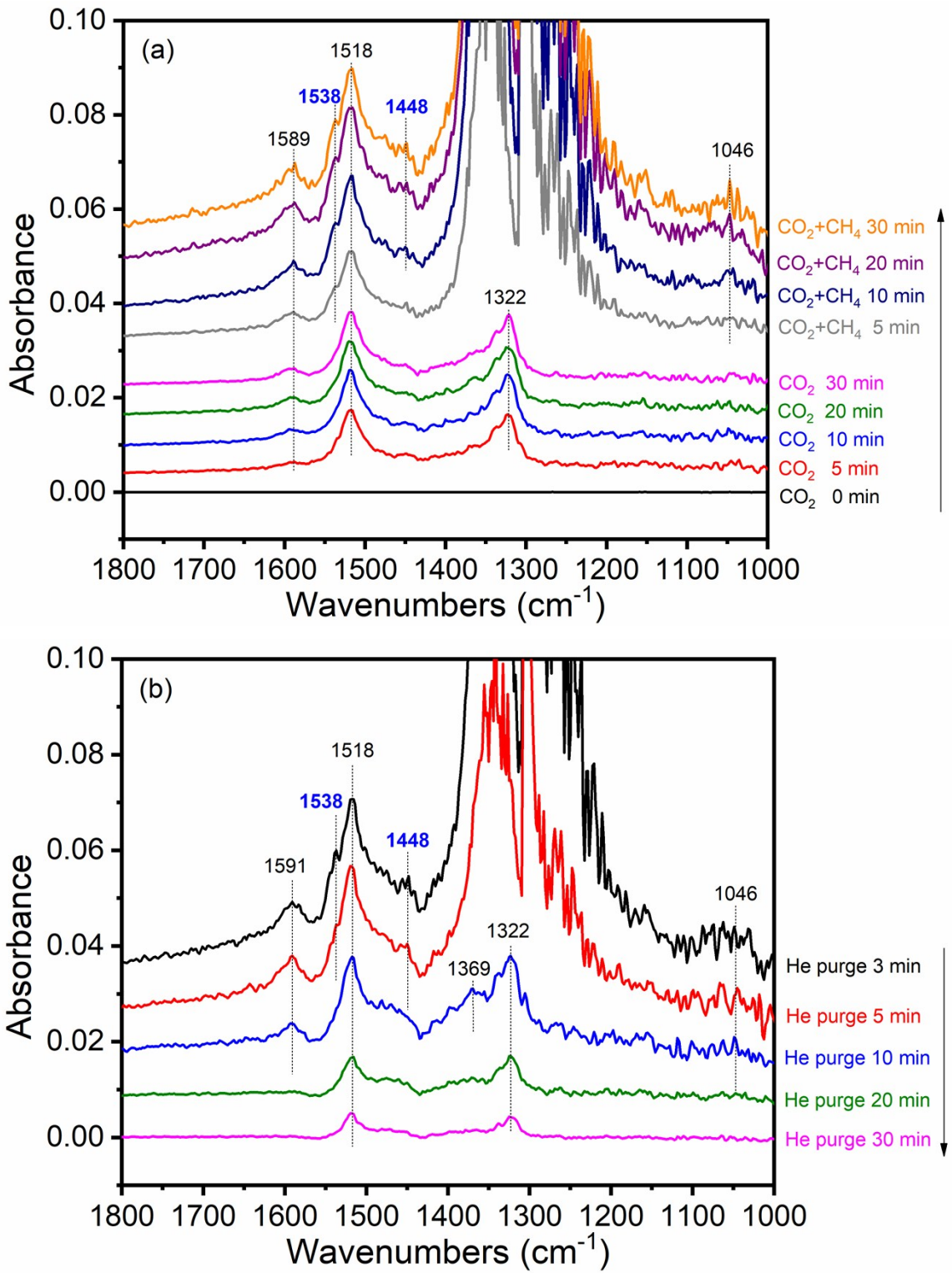

Figure S12. DRIFTS spectra of (a) "CH_4 off−CH_4 on" and (b) He purge obtained over Fe/ZnO at 673 K.

Table S1. The effect of computational methods on the band gap of ZnO, charge transfer in CH_4 dissociation process as well as the energetics associated with CH_4 adsorption and dissociation.

Computational methods	Band gap (eV)	Bader charge transfer (|e|)	E_{ads} (eV)	E_{act} (eV)	E_{rxn} (eV)
PBE+U5.0 (used in paper)	0.92	0.064	-0.06	0.93	0.58
PBE+U7.5	0.63	0.066	-0.06	1.00	0.70
RPBE+U5.0	1.10	0.056	-0.26	1.10	0.65
PW91+U5.0	1.29	0.066	0.19	0.92	0.59

Table S2. Key structural parameters and energies for CH_4 and CO_2 absorption on ZnO($10\bar{1}0$), Fe/ZnO($10\bar{1}0$) and Cu/ZnO($10\bar{1}0$) surfaces (M denotes Zn, Fe or Cu). Corresponding structures refer to Figures 1, S1 and S6.

CH_4 adsorption	ZnO	Fe/ZnO	Cu/ZnO
C_1-M/Å	2.82	2.20	2.40
E_{ads}/eV	-0.06	-0.37	-0.03
E_{ads_disper}/eV	-0.32	-0.58	-0.20
CO_2 adsorption	**ZnO**	**Fe/ZnO**	**Cu/ZnO**
C_2-O_{surf}/Å	1.38	1.38	1.39
O_1-Zn_1/Å	2.09	2.09	2.12
O_2-Zn_2/Å	2.04	2.05	2.06
E_{ads}/eV	-0.83	-0.80	-0.66
E_{ads_disper}/eV	-1.13	-1.06	-0.95

Table S3. Key structural parameters for CH_4 dissociation step on ZnO($10\bar{1}0$), Fe/ZnO($10\bar{1}0$) and Cu/ZnO($10\bar{1}0$) surfaces (M denotes Zn, Fe or Cu). Corresponding structures refer to Figures 1 and S6.

Parameters		C-M/Å	C-H_{diss}/Å	H_{diss}-O_{surf}/Å	H_{diss}-M/Å	H_{diss}-Zn_3/Å
ZnO($10\bar{1}0$)	IS	2.82	1.10	2.46	—	—
	TS	2.14	1.48	1.21	—	—
	FS	1.99	2.44	0.98	—	—
Fe/ZnO($10\bar{1}0$)	IS	2.20	1.13	—	1.91	3.44
	TS	1.95	1.76	—	1.70	1.84
	FS	1.93	2.41	—	1.84	1.52
Cu/ZnO($10\bar{1}0$)	IS	2.40	1.11	—	2.08	3.67
	TS	2.04	1.72	—	1.58	1.96
	FS	2.04	3.41	—	1.61	1.73

Table S4. Key structural parameters for C-C coupling step on ZnO($10\bar{1}0$), Fe/ZnO($10\bar{1}0$) and Cu/ZnO($10\bar{1}0$) surfaces (M denotes Zn, Fe or Cu). Corresponding structures refer to Figures S1 and S6.

Parameters		C_1-C_2/Å	C_2-M/Å	O_2-M/Å	C_1-M/Å	O_1-C_2-O_2/°
ZnO($10\bar{1}0$)	IS	4.10	—	5.39	1.99	129.6
	TS	1.89	—	3.52	2.20	129.6
	FS	1.51	—	2.00	4.26	126.0
Fe/ZnO($10\bar{1}0$)	IS	3.74	3.28	3.14	1.98	128.0
	TS	1.89	1.98	2.01	2.08	133.3
	FS	1.51	2.97	1.87	3.86	124.5
Cu/ZnO($10\bar{1}0$)	IS	4.01	3.31	3.59	2.03	129.1
	TS	2.07	2.37	2.57	2.06	142.8

	FS	1.51	2.87	1.98	3.69	124.2

Table S5. Key structural parameters for H_{diss} migration from initial Zn_3…M to Zn_4…M bridge site on Fe/ZnO($10\bar{1}0$) and Cu/ZnO($10\bar{1}0$) surfaces (M denotes Fe or Cu). Corresponding structures refer to Figures S2(a) and S7(a).

Parameters		C_1-H_{diss}/Å	H_{diss}-M/Å	H_{diss}-Zn_3/Å	H_{diss}-Zn_4/Å
Fe/ZnO($10\bar{1}0$)	IS	2.10	1.60	1.79	4.00
	TS	2.04	1.51	3.37	3.19
	FS	3.23	1.77	5.92	1.64
Cu/ZnO($10\bar{1}0$)	IS	2.41	1.62	1.72	4.11
	TS	2.52	1.54	3.72	2.87
	FS	3.37	1.63	4.40	1.68

Table S6. Key structural parameters for H_{diss} migration step from the Zn_4**…**M bridge site to surface O_3 site on Fe/ZnO($10\bar{1}0$) and Cu/ZnO($10\bar{1}0$) surfaces (M denotes Fe or Cu). Corresponding structures refer to Figures S2(b) and S7(b).

Parameters		H_{diss}-O_3/Å	H_{diss}-M/Å	H_{diss}-Zn_4/Å
Fe/ZnO($10\bar{1}0$)	IS	3.78	1.59	1.76
	TS	1.47	1.64	2.64
	FS	0.98	3.14	3.92
Cu/ZnO($10\bar{1}0$)	IS	3.73	1.60	1.73
	TS	1.54	1.66	2.59
	FS	0.99	2.99	3.97

Table S7. Key structural parameters and energies for CH_3COOH* adsorption on ZnO($10\bar{1}0$), Fe/ZnO($10\bar{1}0$) and Cu/ZnO($10\bar{1}0$) surfaces (M denotes Zn, Fe or Cu). Corresponding structures refer to Figure S3.

Parameters	H_{diss}-O_1/Å	H_{diss}-O_3/Å	O_2-M/Å	O_1-C_2-O_2/°	E_{ads}/eV
ZnO($10\bar{1}0$)	1.18	1.26	1.95	125.9	-1.09
Fe/ZnO($10\bar{1}0$)	1.23	1.27	1.86	124.4	-1.73
Cu/ZnO($10\bar{1}0$)	1.28	1.30	1.88	125.6	-1.40

Table S8. Comparison of activation barriers (eV) of elementary steps involved in acetic acid synthesis from CO_2 and CH_4 on ZnO($10\bar{1}0$), Fe/ZnO($10\bar{1}0$) and Cu/ZnO($10\bar{1}0$) surfaces.

Reactions	Elementary steps	ZnO	Fe/ZnO	Cu/ZnO
Primary Reactions	CH_4* dissociation	0.93	0.30	0.83
	1st H_{diss} migration	—	0.23	0.70
	C-C-coupling	1.46	0.75	1.43
	2nd H_{diss} migration	—	0.99	1.02
	CH_3COO* hydrogenation	0.32	0	0
Side reactions	CO_2* hydrogenation to COOH*	—	1.64	—
	CO_2* hydrogenation to HCOO*	2.44	1.43	1.12
	CH_3* dissociation	—	1.19	—

References

[1] G. Kresse, J. Furthmüller, *Phys. Rev. B* 1996, **54**, 11169-11186.
[2] J. P. Perdew, K. Burke, M. Ernzerhof, *Phys. Rev. Lett.* 1996, **77**, 3865-3868.
[3] P. E. Blöchl, *Phys. Rev. B* 1994, **50**, 17953-17979.
[4] G. Y. Huang, C. Y. Wang, J. T. Wang, *Comput. Phys. Commun.* 2012, **183**, 1749-1752.
[5] S. Grimme, *J. Comput. Chem.* 2004, **25**, 1463-1473.
[6] G. Henkelman, H. Jónsson, *J. Chem. Phys.* 2000, **113**, 9978-9985.

[7] G. Henkelman, A. Arnaldsson, H. Jónsson, *Comput. Mater. Sci.* 2006, **36**, 354-360.
[8] F. Decremps, F. Datchi, A. M. Saitta, A. Polian, S. Pascarelli, A. Di Cicco, J. P. Itié, F. Baudelet, *Phys. Rev. B* 2003, **68**, 104101-104111.
[9] H. L. Zhu, D. R. Yang, H. Zhang, *Inorg. Mater.* 2006, **42**, 1210-1214.
[10] Mora-Fonz, A. L. Shluger, *Adv. Electron. Mater.* 2020, **6**, 1900760-1900771.
[11] L. L.Chen, Y. Y. Cui, Z. H. Xiong, M. B. Zhou, Y. F. Gao, *RSC Adv.* 2019, **9**, 21831-21843.
[12] L. A. Agapito, S. Curtarolo, M. B. Nardelli, *Phys. Rev. X* 2015, **5**, 011006-011022.
[13] S. H. Deng, M. Y. Duan, M. Xu, L. He, *Phys. B* 2011, **406**, 2314-2318.
[14] J. Q. Wen, J. M. Zhang, G. X. Chen, H. Wu, X. Yang, *Phys. E* 2018, **98**, 168-173.
[15] M. H. Liu, Y. W. Chen, X. Liu, J. L. Kuo, M. W. Chu, C. Y. Mou, *ACS Catal.* 2016, **6**, 115-122.